Integration of thalamic and retrosplenial inputs in presubicular layer 3 gates cross-laminar bursting signal to upstream head direction circuit

Authors

Louis Richevaux[1]*, Dongkyun Lim[1], Mérie Nassar[1], Constanze Mauthe[1], Ivan Cohen[3], Nathalie Sol-Foulon[2], Desdemona Fricker[1]*

[1]Université Paris Cité, CNRS, Integrative Neuroscience and Cognition Center, F-75006 Paris, France, [2]Sorbonne Université, INSERM, CNRS, Paris Brain Institute, ICM, Pitié-Salpêtrière Hospital, F-75013 Paris, France, [3]Sorbonne Université, INSERM, CNRS, Neuroscience Paris Seine, Institut de Biologie Paris Seine, F-75005 Paris, France

Correspondence: desdemona.fricker@parisdescartes.fr, louis.richevaux@parisdescartes.fr

Visual abstract

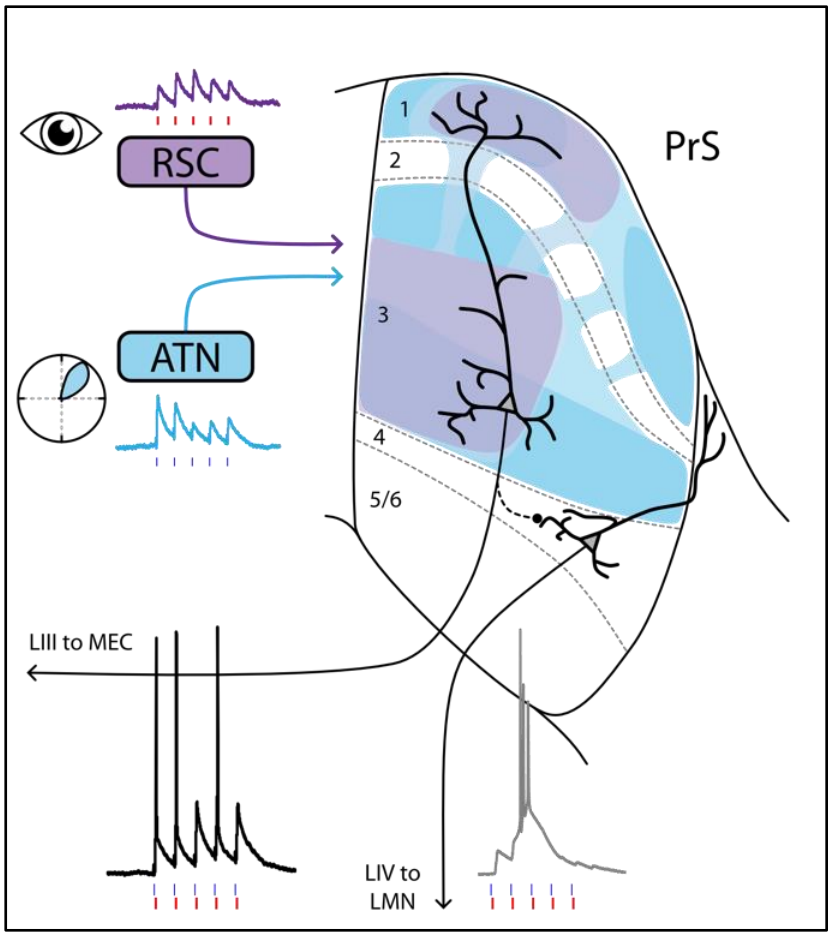

Abstract

Head-direction (HD) signals function as the brain's internal compass. They are organized as an attractor, and anchor to the environment via visual landmarks. This association might happen in the dorsal presubiculum. We find converging monosynaptic excitatory connections from anterior thalamic nucleus and from retrosplenial cortex on single layer 3 presubicular neurons. Independent dual wavelength photostimulation of these inputs in slices leads to action potential generation preferentially for near-coincident inputs, sending an integrated HD signal to medial entorhinal cortex. Layer 4 neurons send their axons to the lateral mammillary nucleus. However, their dendrites avoid overlap with thalamic and retrosplenial axons. Action potentials in layer 4 neurons may be initiated following di-synaptic excitation via layer 3, indicating that landmark updating of HD signals in the lateral mammillary nucleus is a two-step process. Thus, a coherent sense of orientation involves projection specific translaminar processing in the presubiculum.

Introduction

The head direction (HD) system functions as the brain's compass system. It is distributed across several interconnected brain structures, and hierarchically organized from the brainstem to the lateral mammillary nucleus (LMN; (Stackman and Taube, 1998)), the anterior thalamic nuclei (ATN; (Taube, 1995)), and the dorsal Presubiculum (PrS; Ranck, 1984; Taube et al., 1990). Modeling work has postulated that it functions as a ring attractor, where the population of HD neurons is arranged in a one dimensional manifold (Blair and Sharp, 1995; McNaughton et al., 2006; Skaggs et al., 1995). The activity of thalamic and PrS HD neurons is correlated across different brain states, even during sleep, independently of sensory cues (Peyrache et al., 2015). The bump-like activity dynamics of an attractor network can maintain HD signals based on excitatory-excitatory or excitatory-inhibitory interactions (Knierim and Zhang, 2012; Simonnet et al., 2017). However, HD signals may drift in the dark (Taube et al., 1990b; Zugaro et al., 2003). To enable navigation, internally generated information on head direction must be combined with information on location in an environment. Mechanisms underlying the combination of egocentric head direction signals with anchoring to allocentric landmarks remain to be clarified.

The presubiculum is a strong candidate site for the integration of head direction and landmark signals (Jeffery et al., 2016; Yoder et al., 2019). Head direction cells are found in the superficial and deep layers of dorsal presubiculum, also termed postsubiculum (Boccara et al., 2010), and a majority of Layer 3 neurons in the dorsal presubiculum are head direction cells (Preston-Ferrer et al., 2016). These cells receive monosynaptic head direction inputs from the anterior thalamus (Nassar et al., 2018; Peyrache et al., 2015; Balsamo et al., 2022). Lesions of the PrS impair the visual landmark control of a cell's preferred direction in ATN and in LMN (Goodridge and Taube, 1997; Yoder et al., 2015). Presubicular lesions also induce place field instability in the hippocampus (Calton et al., 2003), suggesting this region may have a central role in the anchoring of directionally modulated neurons to environmental landmarks.

Landmark based navigation depends on reliable visual cues. The PrS appears to receive direct

projections from the primary visual cortex and indirect visual input via the retrosplenial cortex (Van Groen & Wyss 2003; Vogt & Miller 1983). The retrosplenial cortex encodes angular head velocity (Alexander & Nitz 2015; Keshavarzi et al. 2022) and visual landmark information (Auger, Mullally, et Maguire 2012; Clark et al. 2010; Sit and Goard 2022). In particular, neurons in the dysgranular retrosplenial cortex encode landmark-dominated head-direction signals (Jacob et al., 2017). Presubicular layer 3 cells receiving projections from both the anterior thalamus and the retrosplenial cortex (Kononenko and Witter 2012) could update the compass and bind landmarks to head direction signals. Presubicular neurons could then broadcast resulting integrated signals directly to the MEC, via deep layers to the ADN and via layer 4 neurons to the LMN (Huang et al., 2017; Yoder et al., 2015; Yoder and Taube, 2011). The different target-specific presubicular projection neurons are well positioned to integrate anterior thalamic and retrosplenial inputs, but technical constraints have limited progress to understand how anatomical inputs translate into functional synaptic integration.

This work was therefore designed to examine integration of visual landmarks and head direction signals in the PrS. Retrograde tracing was used to confirm inputs to the PrS from the ATN and the RSC. The spatial distribution of ATN and RSC targets in the dorsal and ventral PrS was investigated by stereotaxic injection of viral vectors inducing anterograde expression of light-gated ion channels fused to fluorescent reporters. We found that superficial layers of the dorsal PrS are major targets of ATN and RSC projections. We analyzed functional convergence of these inputs in the PrS using dual-wavelength optogenetic stimulations in ex vivo brain slices, while recording from layer 3 and 4 pyramidal neurons. Both ATN and RSC projections made mono-synaptic excitatory connections with single layer 3 principal cells and mostly di-synaptic ones with layer 4 cells. We show that EPSPs induced by ATN and RSC fibers summed non-linearly at short latencies in layer 3 neurons. These data provide initial insights into the integration of landmark and head direction inputs in PrS pyramidal cells.

Methods

KEY RESOURCES TABLE

REAGENT or RESOURCE	SOURCE	IDENTIFIER
Bacterial and virus strains		
AAV5.Syn.Chronos-GFP.WPRE.bGH	Addgene	59170P
AAV5.Syn.ChrimsonR-tdTomato.WPRE.bGH	Addgene	59171P
pAAVretro-CAG-tdTomato	Addgene	59462P
Chemicals, peptides, and recombinant proteins		
Retrobeads	Lumafluor	Red Retrobeads™
Streptavidin, Alexa Fluor™ 647 Conjugate	Thermofisher Scientific	S32357
Experimental models: Organisms/strains		
C57BL/6J	Janvier Labs	https://janvier-labs.com/fiche_produit/2-c57bl-6jrj/
Software and algorithms		
MATLAB	MathWorks	https://www.mathworks.com/
pClamp	Molecular devices	RRID:SCR_011323
AxoGraphX	Axograph	https://axograph.com
Other		
Prolong Gold antifade mountant	Invitrogen	Cat#P36930; RRID:SCR_015961

RESOURCE AVAILABILITY

Lead contact

Further information and requests should be directed to the lead contact, Desdemona Fricker (desdemona.fricker@parisdescartes.fr).

Materials availability

This study did not generate new unique reagents.

EXPERIMENTAL MODEL AND SUBJECT DETAILS

Animals

Experiments were performed on wild-type and transgenic C57Bl6 mice, housed on a 12 hours

light/dark cycle with food and water available *ad libitum*. Animal care and use conformed to the European Community Council Directive (2010/63/EU) and French law (87/848). Our study was approved by the local ethics committee (CEEA - 34) and the French Ministry for Research 01025.02.

METHOD DETAILS

Viral vectors and beads

Projecting neurons were labeled with retrograde fluorescent tracers (Retrobeads, Lumafluor, and pAAV-CAG-tdTomato, Addgene 59462P). Fluorescent beads were stored at 4°C before use. Channelrhodopsin expression was induced by injecting Adeno-associated viral constructions. AAV5.Syn.Chronos-GFP.WPRE.bGH (AAV5-Chronos, Penn Vector Core, Addgene 59170P) was used to induce neuronal expression of the blue light induced channelrhodopsin Chronos fused to the GFP marker and under the control of the Synapsin promoter. AAV5.Syn.ChrimsonR-tdTomato.WPRE.bGH (AAV5-Chrimson, Penn Vector Core, Addgene 59171P) induced neuronal expression of the red light gated channelrhodopsin Chrimson fused to the tdTomato marker, under the control of the Synapsin promoter. Viral vectors were stored at -80°C before use.

Stereotaxic surgery

Mice at ages of 4-5 weeks were anesthetized by intraperitoneal (i.p.) injection of a mixture of ketamine hydrochloride and xylazine (100 and 15 mg/kg respectively, in NaCl 0.9%). They were placed in a stereotaxic frame for injections. Fluorescent beads for retrograde tracing were injected (300-500 nl) into the PrS at the coordinates: -4.06 antero-posterior (AP), 2.00 medio-lateral (ML) and -2.15 mm dorso-ventral (DV) and into the LMN (-2.8 AP, 0.75 ML, -5.35 DV) with respect to the bregma.
Viral injections were performed unilaterally (Mathon et al., 2015; Richevaux et al., 2019) at the coordinates -0.82 AP, 0.75 ML and -3.2 mm DV for the ADN, and at -2.1 to -2.15 AP, 0.65 ML and -0.65 mm DV for the RSC. Volumes of 200 to 250 nl were injected with a 10 µL Hamilton syringe equipped with 33ga needle over a time of 10 min. The needle was slowly removed after a delay of 10 min to avoid leakage from the injection site. Best expression for AAV5 serotypes was achieved after 3 to 4 weeks.

Tissue fixation and slicing for retrograde tracing

Brains were extracted 4 days after retrobead injection. Mice were anesthetized by i.p. injection of the ketamine/xylazine mixture. An intracardiac perfusion with 0.1M PBS was followed by perfusion with 4% paraformaldehyde. Brains were then removed, stored overnight in paraformaldehyde at 4°C and then washed in PBS. Coronal or horizontal sections were cut at 100 µm with a vibratome and stored in sucrose at 4°C.

Preparation of brain slices for physiology

Slices of the temporal lobe were prepared 3-4 weeks after injection of AAV5 viral constructions. Mice were anesthetized by i.p. injection of the ketamine/xylazine mixture. They were then perfused intracardially with a cutting solution containing (in mM): 125 NaCl, 25 sucrose, 2.5 KCl, 25 $NaHCO_3$, 1.25 NaH_2PO_4, 2.5 D-glucose, 0.1 $CaCl_2$, 7 $MgCl_2$, cooled to 4°C, and oxygenated with a 5% CO_2 / 95% O_2. The brain was removed and a vibratome was used to cut horizontal slices at 300 µm in the same solution. Slices were stored for 15 min at 34°C in an ACSF containing (in mM): 124 NaCl, 2.5 KCl, 26 $NaHCO_3$, 1 NaH_2PO_4, 2 $CaCl_2$, 2 $MgCl_2$, and 11 D-glucose, bubbled with 5% CO_2 / 95% O_2. They

were then kept in the same solution at room temperature until recording.

Whole-cell patch-clamp recordings

Slices were transferred to a recording chamber perfused with oxygenated, warmed (~32 °C) ACSF and mounted on an epifluorescence microscope. Patch-clamp records were made from neurons with borosilicate glass pipettes of external diameter 1.5 mm (Clark Capillary Glass, Harvard Apparatus) pulled with a Brown-Flaming electrode puller (Sutter Instruments). Electrodes, filled with a potassium-gluconate based solution containing (in mM): 135 K-gluconate, 1.2 KCl, 10 HEPES, 0.2 EGTA, 2 $MgCl_2$, 4 MgATP, 0.4 Tris-GTP and 10 Na_2-phosphocreatine, had a resistance of 4-8 MΩ. An alternative, cesium-gluconate based solution facilitated neuronal depolarization to examine synaptic inhibition. It contained (in mM): 125 Cs-gluconate, 10 HEPES, 0.2 EGTA, 2 $MgCl_2$, 4 MgATP, 0.4 Tris-GTP and 10 Na_2-Phosphocreatine, together with 5 mM QX-314 to block Na^+ channels. Pipette solutions also contained 3 mM biocytin to reveal morphology after recording. They were adjusted to pH 7.3 and osmolarity 290 mOsm. Whole-cell patch-clamp signals were filtered at 3kHz, amplified with a MultiClamp 700B amplifier and acquired with pCLAMP software (Molecular Devices). Monosynaptic excitation induced by optical stimulation was tested in the presence of TTX (1 µM) and 4-AP (100 µM). NBQX (10 µM) and APV (100 µM) were used to block AMPA and NMDA receptors respectively. Gabazine (10 µM) was used to block $GABA_A$ receptors.

Optical stimulation

LED illumination (Cairn Research, OptoLED) was used to detect expression of the fluorescent reporters GFP and tdTomato, and to stimulate opsin-expressing axons in the presubiculum. They were stimulated using a 470 nm LED for Chronos and a 627 nm LED for Chrimson. Illuminated spots had a diameter of 200 µm with a 60x objective and were centered on the recorded cell soma. Photostimulation thus covered most of the basilar dendrites of layer 3 pyramidal neurons (typical size from tip of apical to tip of basilar dendrite <400µm). Stimulations consisted of light pulses of 0.5 to 5 ms duration, repeated 5-10 times at 20 Hz.

A multiband filter allowed simultaneous stimulation by blue and red LEDs of axons containing Chronos and Chrimson (Simonnet et al., 2021). Stimulus power intensity (set in mV) was calibrated as light intensity. The response probability of layer 3 cells was calibrated to blue or red illumination of ATN or RSC afferents expressing Chronos or Chrimson to avoid stimulus overlap (see Supp. Fig. 5, 6). Chronos was targeted to the ATN and Chrimson to the RSC after testing the reverse configuration. Projections from the thalamus are larger and Chronos is more sensitive to blue light, so this configuration assured reliable activation of thalamic fibers at minimal blue-light intensities. For experiments investigating the integration of ATN and RSC inputs, we aimed to give roughly equal weights to both inputs: Chrimson-expressing fibers were stimulated with light of intensity adjusted to initiate optically evoked excitatory postsynaptic potentials (oEPSPs) of amplitude similar to those induced by blue light Chronos-fiber stimuli.

Data analysis

ATN and RSC projections to the PrS, were analyzed from Chronos and Chrimson expression, using the ImageJ Plot Profile plug-in to quantitate normalized plot profiles (2000 pixels) of horizontal presubicular sections. Dorso-ventral differences were derived by dividing differences in labeling intensity between the PrS and the dentate gyrus (DG) molecular layer by DG intensity in slices from 5 dorso-ventral PrS levels. Values from all animals were averaged and then normalized.

Cells were qualified as synaptically 'connected' when they responded to light stimulation of afferent axons with a delay < 8 ms. Slices with very low or absent expression of the fluorescent reporter were excluded. Cells were qualified as 'non-connected' synaptically, if they did not respond to light stimulation, but at least one neighboring cell in the same slice did.

Intrinsic neuronal properties were analyzed with custom MATLAB routines to derive 15 electrophysiological parameters (Huang et al., 2017). Parameters were standardized and unsupervised cluster analysis performed with MATLAB was used to compare different neurons (Huang et al., 2017; Simonnet et al., 2013).

Axograph was used to analyze neuronal responses to optical stimulation of ATN and RSC fibers. Layer 3 neurons were recorded at potentials near -65 mV. Responses to light were averaged from 10 stimulus trains at 20 Hz. Amplitudes and latencies of initial light evoked EPSCs, of latency shorter than 10ms, were quantified from voltage-clamp records. Latency was measured from stimulus onset to 10% of the peak amplitude of the first optically induced EPSC. Amplitude was measured with respect to the pre-stimulus baseline. Paired-pulse ratio (PPR) was defined as the ratio of the amplitude of the second to the first EPSC and 10/1 ratio as that between the 10th and the 1st EPSC, both from responses to 20 Hz stimulations. Spike probability was counted over 5 to 10 trials per cell and then averaged over all cells. EPSPs induced by dual wavelength stimulation were analyzed using Axograph and a custom-made software. Events evoked by light stimuli were detected in a window of 1-10 ms after stimulation. EPSP amplitude and integrated area were calculated over 50 ms after stimulation. Baseline suppression was applied using an average of membrane potential during 50 ms before stimulation. Summation of ATN and RSC evoked EPSCs in layer 3 neurons was determined from the amplitude and integral of averaged events. Summation was considered to be supralinear, if values were more than 10% higher than a linear addition, linear for values within ± 10%, and sublinear for values more than 10% lower.

Biocytin revelation and morphology

Recorded neurons were filled with biocytin to visualize their morphology and location. Slices were fixed in 4% PFA in 0.1 M PBS at 4°C overnight, washed 3 times in 0.1 PBS and cryoprotected in 30% sucrose. Cell membranes were permeabilized by three freeze-thaw cycles over dry ice and rinsed in PBS. Slices were agitated in a saturation buffer (2% milk, 1% Triton X-100 in 0.1 M PBS) for 2 hours at room temperature. They were then incubated with Streptavidin-Cy5 conjugate (1:500) and DAPI (1:1000) overnight at 4°C. Sections were washed 3 times with PBS and mounted on coverslips with ProLong gold antifade mountant. For anatomical study they were mounted in Mowiol medium. Cell, bead and virus expression were visualized with an epifluorescence microscope. Higher resolution of morphology was obtained with confocal microscopy. The cell shown in Fig. 4 was reconstructed with Neurolucida software and those in Fig. 7 using IMARIS.

QUANTIFICATION AND STATISTICAL ANALYSIS

Data was analyzed with AxoGraphX and custom-written software (MATLAB, The MathWorks). Results are given as mean ± SEM. Statistical analysis was performed with Prism (GraphPad Software). The Mann-Whitney unpaired t-test was used to compare two groups. The Wilcoxon or Kruskal-Wallis test was used to compare paired groups. Evolution of parameters evoked by optical stimulation (current or potential amplitudes, spike probability) was analyzed with Friedman's test followed by multiple comparison Dunn's test. Šidák's multiple comparison test was also used to compare linear and observed responses to ATN and RSC stimulations. Significance levels are given as p values.

Results

ATN and RSC send strong axonal projections to the dorsal Presubiculum

The origins of the main afferents projecting to the presubiculum were explored by injecting retrogradely transported fluorescent beads into the PrS (Fig. 1A). After 4 days, coronal slices were prepared to examine the injection site and transport of the beads. Some beads remained close to the PrS injection site, due in part to local projections. Strong bead signals were detected within the two subnuclei that form the anterior thalamus, the anterodorsal (AD) and anteroventral (AV) part of ATN. Neurons in AD were labeled most strongly in the medial portion of the AD, while labeled neurons in AV were found in its lateral portion (Fig. 1B). Many neurons in the RSC were labeled. Cells with somata in layers 2 and 5 of the dysgranular dRSC were labeled, while mostly layer 5 cells of granular gRSC contained beads (Fig. 1C). Regions adjacent to the presubiculum including the subiculum (Sub), parasubiculum (PaS) and the medial and lateral entorhinal cortices (MEC, LEC) were labeled as was the contralateral PrS. Beads were also detected in the laterodorsal thalamic nucleus (LD). Table S1 summarizes these data, indicating some labeling also in the visual cortices, perirhinal cortex, the nucleus reuniens of the thalamus, the dorsolateral geniculate nucleus, and the claustrum. Some beads were observed in the CA1 region, which has not previously been reported. Potentially though, this labeling could derive from a bead leak into the nearby PaS which is innervated by CA1 (Van Groen et Wyss 1990a). In summary, the ATN and RSC are the major regions projecting to the presubiculum with lesser inputs from other sites.

Projections from the ATN or RSC to the presubiculum were explored by injecting at these sites an anterogradely transported viral construct which expressed the modified Channelrhodopsin Chronos fused to GFP (Fig. 1D). After 4 weeks, horizontal slices were prepared to verify the ATN injection site. Chronos-GFP labeling was mostly confined to the ATN, occasionally extending to medial thalamic and reticular nuclei nearby, possibly as bundles of projecting fibers (Fig. 1E, Supp. Fig. 1). As for the RSC injection site, coronal sections (Fig. 2F) showed strong expression in layer 5, especially deeper zones, and layer 6 of both dysgranular and granular RSC, while labeled dendrites were evident in layer 1. Chronos-GFP expression extended throughout the RSC, from -1.7 to -3.7 posterior to Bregma on the antero-posterior axis (Supp. Fig. 2).

Projections of the ATN to the presubiculum were examined in horizontal sections (Fig. 1G). ATN axons expressing the Chronos-GFP construct targeted layers 1 and 3 of the presubiculum, avoiding layer 2 (Simonnet et al., 2017; Nassar et al., 2018). Labeling was very precisely limited to the presubiculum. We found a sharp drop of green fluorescence at the posterior border with the parasubiculum, the anterior border with the subiculum and the lateral border with deep layers. Axon terminals in layer 3 were not homogeneously distributed. Patches of higher density were evident in deep layer 3 (Fig. 1G). Along the dorso-ventral axis, ATN axons projected from -2 to -4 mm ventral to Bregma. Fluorescence was not detected in adjacent regions including the Sub, PaS, and DG. We noted that ATN axons avoided patches of calbindin positive neurons, located in anterior layer 2, that project to contralateral PrS (Preston-Ferrer et al. 2016; Fig. 1K).

RSC projections to the presubiculum (Fig. 1H), traced with the fluorescent Chronos-GFP construct, also projected to layers 1 and 3. Unlike ATN axons, they were restricted to dorsal regions of the presubiculum (from -2 to -3 mm ventrally to Bregma on the dorso-ventral axis)(Fig. 1H, I, J). RSC axon labeling tended to avoid the ATN patches (Fig. 1G, K. Fig. 3). Overall, these data show ATN and RSC afferents innervate overlapping regions in the dorsal part of the PrS, in layer 1 and deep parts of

layer 3. Different spatial patterns of fiber terminations suggest distinct local connectivities.

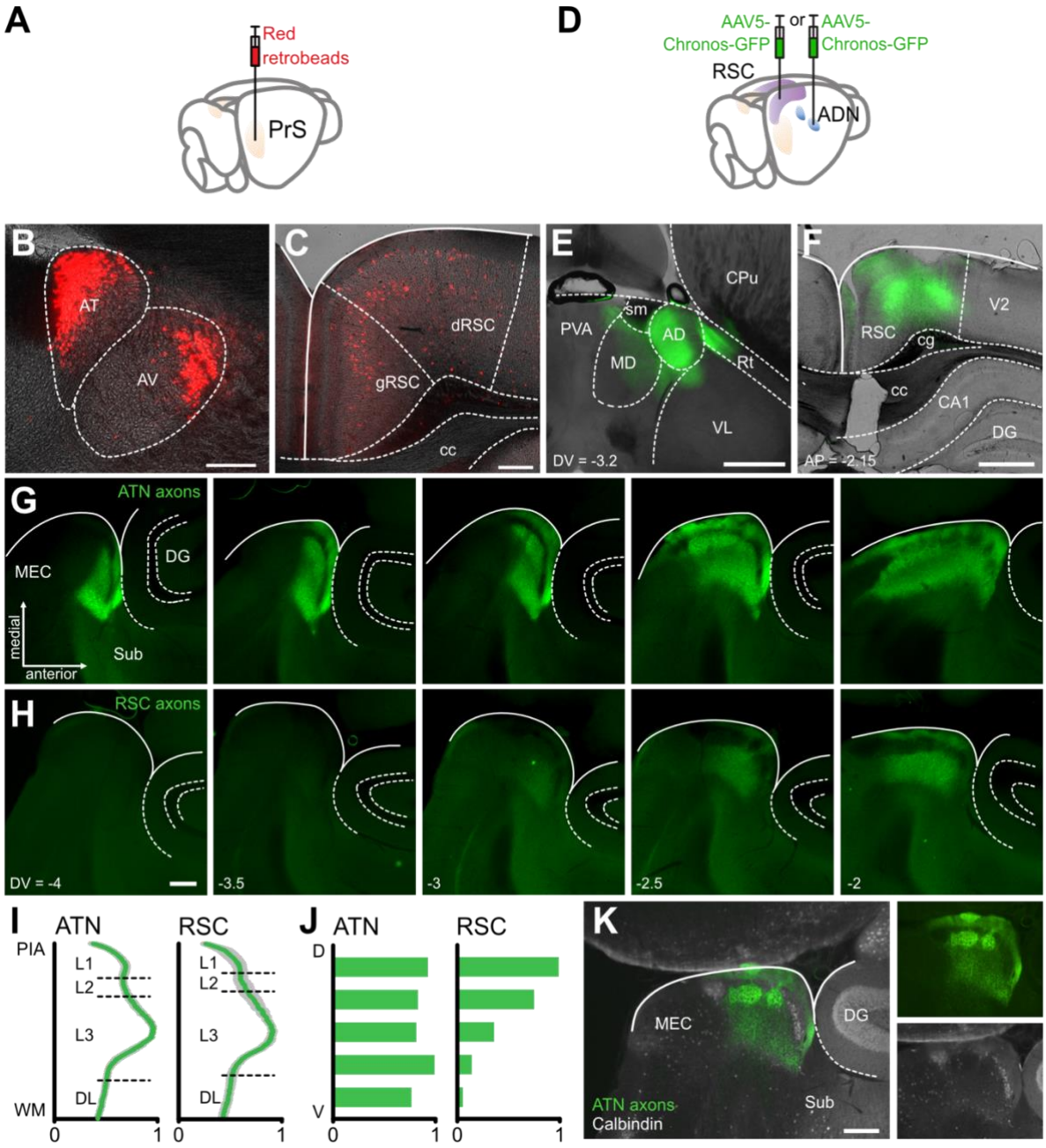

Figure 1. ATN and RSC send strong axonal projections to the superficial layers of dorsal Presubiculum

A, Retrograde labeling of cortical and subcortical regions projecting to the presubiculum (PrS) with retrobeads.

B, Ipsilateral anterodorsal and anteroventral thalamic nuclei are labeled with beads.

C, Ipsilateral granular (gRSC) and dysgranular (dRSC) retrosplenial cortex labeling. Scale bars B, C 200 µm.

D, Anterograde labeling of thalamic and retrosplenial projections to PrS with AAV-Chronos-GFP.

E, F, Injection sites in ATN (E) and RSC (F). AD: anterodorsal thalamic nucleus, AV: anteroventral thalamic nucleus, CA1: field of the hippocampus, cc: corpus callosum, cg: cingulum, CPu: caudate putamen, DG: dentate gyrus, MD: thalamic medial dorsal nucleus, MEC: medial entorhinal cortex, PaS: parasubiculum, PVA: paraventricular thalamic nucleus, anterior, Rt: thalamic reticular nucleus, sm: stria medullaris, Sub: subiculum, VL: thalamic ventrolateral nucleus.

G, H, Five sequential 100-µm horizontal slices of the parahippocampal region show ATN (G) and RSC (H) axons expressing Chronos-GFP (green). Dashed lines show limits of the parahippocampal region to the left and of the

dentate gyrus to the right. Dorsoventral level with respect to bregma. Scale bars 100 µm.
I, Normalized profiles of fluorescent intensity for ATN and RSC projections to the presubiculum, from white matter (WM) to pia (PIA). Mean (green) ± SEM (grey), n = 8.
J, Ventral (V) to dorsal (D) normalized distribution of ATN and RSC projections to the presubiculum, n = 3 mice.
K, ATN axon labeling is segregated from calbindin labeling in the PrS. Scale bar 100 µm.

Layer 3 neurons receive direct excitation from both the ATN and RSC

We next examined the effects of ATN and RSC afferents on pyramidal cells of the PrS layer 3 (Rees et al., 2017). Responses to photo-stimulation of the Chronos-GFP construct injected either in the thalamus or in the retrosplenial cortex (Fig. 2A) were recorded in layer 3 neurons (Fig. 2B). These cells had robust regular firing patterns in response to depolarizing current injections (Fig. 2C). Their intrinsic properties were rather uniform (Table S2) and an unsupervised cluster analysis suggested they formed a single population (Fig. 2D).

Blue light activation of either ATN or RSC axons expressing Chronos-GFP reliably evoked synaptic responses in whole-cell patch-clamp records from layer 3 cells. High intensity stimulation (1 - 3 mW) evoked EPSCs or EPSPs with a probability of 84% (70/83) for ATN fibers and 85% (104/123) for RSC fibers (Fig. 2E). Excitatory postsynaptic currents or potentials evoked by optical stimulation of thalamic and retrosplenial inputs will be referred to as oEPSCs and oEPSPs. Mean oEPSC amplitudes (Fig. 2F) were similar for ATN (-305.0 ± 61.0 pA, n = 24) and RSC fiber stimuli (-305.8 ± 59.1 pA, n = 27). Response latency (Fig. 2G) to ATN axon stimulation was 2.45 ± 0.19 ms (n = 24) and that for RSC axon stimulation was 2.93 ± 0.23 ms (n = 27). The variability in latency of oEPSCs (Supp. Fig. 3A, B) induced by RSC afferent stimuli was 0.35 ± 0.09 ms (n = 27) and that for oEPSCs induced by ATN stimuli was 0.19 ± 0.06 ms (n = 24). These short oEPSC latencies suggest monosynaptic transmission. We confirmed this point by showing that oEPSCs were maintained in presence of TTX (1µM) and 4AP (100µM) (Fig. 2H, n = 2 and 12 for ATN and RSC respectively). EPSCs induced by stimulation of ATN and RSC fibers were reduced in amplitude and decayed more quickly in the presence of the NMDA receptor antagonist APV (50 µM) and were completely abolished by the AMPA receptor antagonist NBQX (1 mM) (Fig. 2I). The shape of oEPSCs induced by light stimulation of ATN and RSC fibers was comparable. Rise times (Supp. Fig. 3C-E) were 1.38 ± 0.15 ms for ATN EPSCs (n = 15) and 1.38 ± 0.08 ms for RSC-mediated EPSCs (n = 15) and mean half-widths were 4.00 ± 1.02 ms for ATN-induced ESPCs (n = 15) and 4.34 ± 1.18 ms for RSC EPSCs (n = 15). The mean time constant (tau decay) for ATN-mediated EPSCs was 3.01 ± 0.21 (n = 15) and for RSC-induced EPSCs 3.17 ± 0.27 (n = 15).

Optical stimulation of ATN and RSC fibers at lower light intensities elicited sub-threshold synaptic events in layer 3 cells. oEPSP amplitude for ATN mediated events was 4.09 ± 1.18 mV (n = 11) and for RSC events it was 4.80 ± 0.84 mV (n = 11). Maximal slopes were 2.93 ± 0.82 V/s for ATN-mediated events (n = 11) and 3.02 ± 0.53 V/s for RSC EPSPs (n = 11), while time constants were 81.4 ± 11.6 for ATN EPSPs (n=11) and 86.9 ± 11.2 ms for RSC EPSPs (n = 11). Rise times were shorter for subthreshold EPSPs induced by ATN afferents at 3.00 ± 0.24 ms (n = 11) while those for RSC initiated EPSPs were 3.59 ± 0.34 (n = 11, p = 0.042, Wilcoxon test; Supp. Fig. 4A-E). These data show that ATN and RSC axons make monosynaptic, glutamatergic excitatory contacts on layer 3 PrS cells.

The dynamics of responses to repetitive stimulation of layer 3 PrS cells were tested using 20 Hz trains of light stimuli to activate ATN or RSC afferents. oEPSCs for both inputs followed depressing kinetics in records from neurons of different mice. Amplitude decreased for both inputs (Fig. 2J, K), significantly after the fourth pulse (Friedman's test and Dunn's multiple comparison test). The *10/1*

ratio was significantly lower than the paired-pulse ratio (PPR) in both cases (ATN *10/1* 0.56 ± 0.05 vs PPR 0.86 ± 0.05, n = 15, p < 0.0001, Wilcoxon test, RSC *10/1* 0.64 ± 0.05 vs PPR 0.83 ± 0.03, n = 15, Wilcoxon test) (Fig 2L). ATN fiber stimulation induced PrS cell firing in current-clamp with a high probability for initial stimuli and lower stable probabilities for later stimuli in the train. Similarly, 20 Hz stimulation of RSC afferents evoked spikes with high probability for initial stimuli followed by decreasing probability for later stimuli (on fourth and 7^{th}-10^{th} pulses, Friedman's and Dunn's multiple comparison tests) (Fig. 2M, N). Subthreshold stimulations had similar dynamics (Fig. 2O). Stimulation with lower light intensities (< 1 mW) to initiate sub-threshold oEPSPs elicited different dynamic responses. ATN afferent trains elicited responses with depressing dynamics: the amplitude of the fifth oEPSP was significantly less than the first one (3.18 ± 0.88 vs 5.11 ± 1.64 mV, p = 0.0185, Friedman's and Dunn's tests). In contrast, little or no oEPSP depression was detected for subthreshold responses to 20 Hz stimulation of RSC afferents (Supp Fig. 4F-H). These data reveal distinct patterns of integration of repetitive activity in glutamatergic ATN and RSC afferents terminating on PrS layer 3 pyramidal cells.

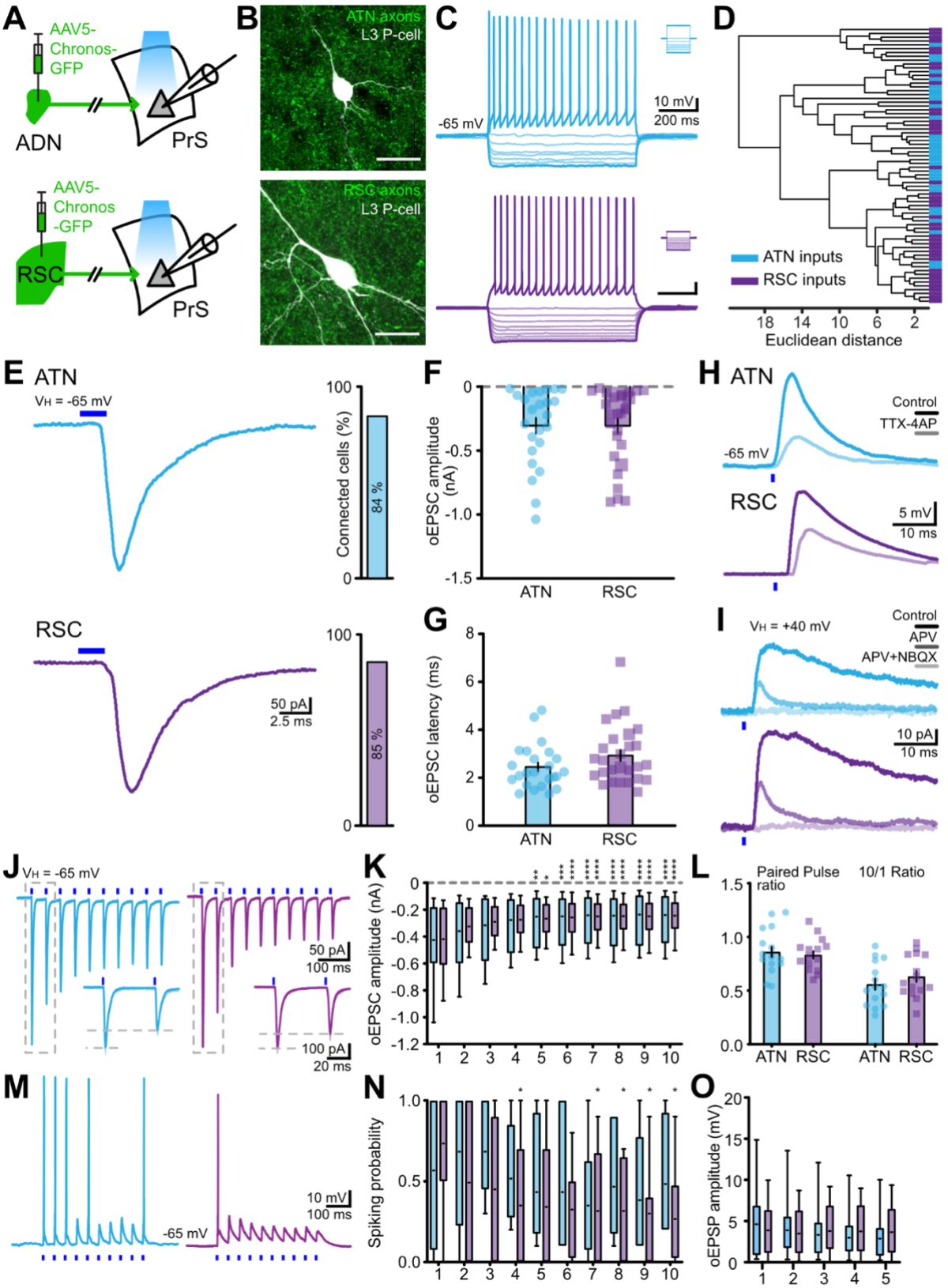

Figure 2. Responses of layer 3 presubicular cells to activation of ATN and RSC fibers.

A, Experimental design. AAV5-Chronos is stereotaxically injected into ATN or RSC

B, Biocytin labeled layer 3 cells and GFP positive axons from the ATN or RSC. Scale bar 10 µm.

C, Firing pattern of two layer 3 cells receiving inputs from the ATN (*cerulean*) and the RSC (*purple*).Insets show current commands.

D, Cluster analysis of physiological parameters for cells tested by stimulating ATN or RSC fibers.

E, Representative EPSCs evoked in layer 3 cells by light stimulation (blue bar) of ATN or RSC inputs. Right, proportion of cells receiving ATN or RSC inputs.
F, Average amplitudes of ATN and RSC induced synaptic currents.
G, Latency of EPSCs evoked by light-stimulation of ATN (n = 24 cells) or RSC fibers (n = 27 cells).
H, EPSPs induced in layer 3 cells by stimulating ATN or RSC inputs in absence and presence of 1 µM TTX and 100 µM 4-AP in single traces.
I, EPSCs induced by stimulating ATN or RSC fibers in the absence and presence of 100 µM APV and 10 µM NBQX. Holding potential +40 mV.
J, Voltage-clamp responses of layer 3 cells to 20 Hz train stimulations of ATN (*left*) and RSC (*right*) inputs. Insets show EPSCs in response to the first two stimuli.
K, oEPSC amplitudes for 10 ATN or RSC fiber stimuli at 20 Hz. n = 15 neurons. Short middle line, mean; Min to max and quartiles.
L, Paired-pulse ratio (PPR) and 10/1 ratio (ratio between 10^{th} and 1^{st} event amplitudes) for ATN or RSC inputs. Wilcoxon matched-pairs signed rank test: ATN PPR vs 10/1 **** $p < 0.0001$, RSC PPR vs 10/1 *** $p = 0.0001$.
M, Current clamp traces. Action potentials and EPSPs evoked by 10 stimuli at 20 Hz.
N, Spiking probability during trains of 10 stimuli. ATN, n = 6, RSC, n = 12. Full line, median; short line, mean; Min to max and quartiles. In K and N, * $p < 0.05$, ** $p < 0.01$, *** $p < 0.001$, **** $p < 0.0001$ from Friedman's test followed by Dunn's *post-hoc* test.
O, oEPSPs amplitude for trains of 5 stimulations at 20 Hz.

Convergence of ATN and RSC inputs on single layer 3 neurons

Are single layer 3 pyramidal cells innervated by both ATN and RSC afferents? It seemed likely since the probability of connection to a given cell was 84% for ATN fibers and 85% for RSC afferents. Cluster analysis (Fig. 2D) provided no evidence for subpopulations of layer 3 cells (but see Balsamo et al., 2022). We tested the hypothesis by independent activation of ATN and RSC afferents using photostimulation at two different light frequencies.

A potential difficulty with this approach is the existence of an overlap in the excitation spectra of blue-light activated Chronos (400-600 nm) and the red-light activated Chrimson (450-700 nm; Klapoetke et al., 2014). Excitation of Chronos with high intensities of blue light might also excite Chrimson. Stimulating with red light at 630 nm should elicit neurotransmitter release in Chrimson-containing but not Chronos-expressing fibers, which we found was indeed the case (Supp. Fig. 6A). Blue light stimuli at 470 nm and intensities higher than 0.01 mW elicited oEPSPs in layer 3 cells of animals with Chronos-expressing fibers. In contrast, blue light intensities higher than 0.25 mW were needed to induce oEPSPs in different animals with Chrimson-expressing axons (Supp. Fig. 5, 6B). Moreover, the amplitude of these events was smaller in Chrimson-injected than in Chronos-injected mice. Thus, in our experimental conditions, blue light intensities up to 0.25 mW could be used to excite Chronos-positive axons with confidence that Chrimson-expressing fibers would not be stimulated.

We also tested the inverse, red light component of the dual stimulus strategy. Intensities were tested in mice injected either with AAV5-Chronos to label ATN fibers or AAV5-Chrimson to label RSC afferents. The strategy was validated by showing that red light induced oEPSPs in Chrimson-containing, but not Chronos-expressing fibers, while blue light evoked synaptic events in Chronos-, but not Chrimson-expressing fibers (Supp. Fig. 6C-H, Supp. Table 3).

Injection in the same animal of the Chronos construction to the thalamus and that for Chrimson to the retrosplenial cortex permitted visualization of ATN and RSC afferents to the

presubiculum (Fig. 3A, B). When the constructions were expressed, ATN and RSC axon terminals could be visualized in dorsal presubicular superficial layers (cf. Fig. 1). Layer specificities, and labeling inhomogeneities were apparent as were high density ATN patches below layer 2 with no RSC axon innervation (Fig. 3B). With apical dendrites in layer 1 and basilar dendrites in layer 3, layer 3 PrS pyramidal cells might be innervated by ATN and RSC axons in both layers (Fig. 3D). Indeed, optical stimulation of ATN and RSC axons, evoked synaptic responses in current-clamp and voltage-clamp in 14 out of 17 layer 3 pyramidal cells tested (Fig. 3E, F).

We searched for an anatomical substrate of this innervation. Labeled ATN or RSC terminals close to the dendrites (< 1µm) of biocytin filled layer 3 pyramidal cells were quantified (n = 6 cells; Fig. 3G). The distribution of potential contact sites on dendritic trees of layer 3 neurons was diverse. Some neurons exhibited highly segregated domains receiving either ATN or RSC inputs. Cell 1 had a high proportion of clustered RSC putative synapses on its apical tuft while basilar dendrites were mostly surrounded by potential thalamic terminals. In cell 2, RSC terminals were clustered close to apical dendrites and also together with ATN terminals close to basilar dendrites. In contrast, many ATN terminals were located closer to apical dendrites of cell 3. While the segregation of RSC inputs in apical dendrites and thalamic inputs to basal dendrites might favor supralinearity, the distribution of afferent terminals differed between neurons, and we did not find a clear pattern with relation to the linearity scores (cell 1, supralinear (1.39); cell 2, roughly linear (0.91); cell 3, sublinear score (0.69), Fig. 3G, H). Beside this, we noticed that certain synapses could be located close to each other (< 20 µm) on single dendrites as shown in Fig. 3I. This could open the possibility for local dendritic computations and supra-linearities. Synaptic clustering has been associated with local NMDA-mediated dendritic spikes which could contribute to non-linear summation of synaptic events (Larkum et al., 1999, 2007, 2009).

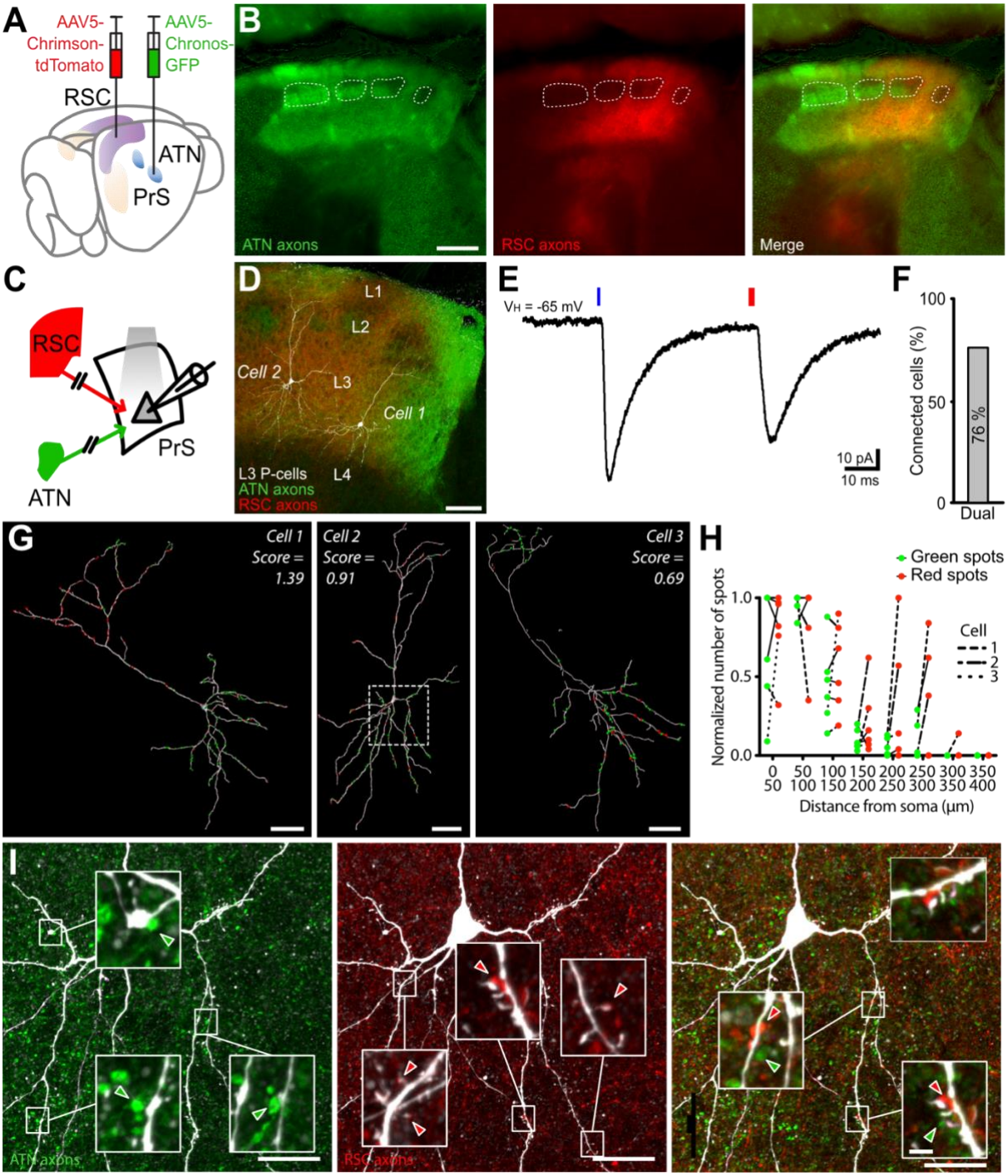

Figure 3. Opsin expressing ATN and RSC axons contact single L3 pyramidal neurons in dorsal presubiculum.

A, Experimental design. AAV5-Chronos-GFP and AAV5-Chrimson-tdTom are injected into ATN and RSC respectively.

B, Axons from ATN (green) and RSC (red) in superficial layers of dorsal presubiculum. RSC fibers avoid patch-like microstructures formed by ATN fibers in upper layer 3. Scale bar, 200 µm.

C, Presubicular layer 3 cells recorded in double injected mice.

D, Two biocytin labeled PrS layer 3 pyramidal cells surrounded by ATN (green) and RSC (red) axons.

E, EPSCs evoked by photostimulation of either ATN (blue light) or RSC fibers (red light).

F, 13/17 (76%) of layer 3 pyramidal neurons receive synaptic inputs from both ATN and RSC afferents.

G, Distributions of putative ATN (green) and RSC (red) synapses on the dendrites of three layer 3 neurons. The linearity score is indicated. Scale bar 50 µm. The dotted square area on Cell 2 is enlarged in panel I.

H, Normalized number of green and red spots for 6 neurons as a function of the distance from soma. Paired values are indicated by dotted lines for the 3 cells in G.
I, Examples of ATN-labeled (left), RSC-labeled (middle) and both (right) synapses closely apposed to dendrites of a biocytin-filled layer 3 pyramidal cell. Scale bar 20 µm. Insets show enlarged views. Scale bar 2µm.

Supralinear subthreshold integration and amplification of ATN and RSC excitatory postsynaptic potentials

The ability to independently stimulate ATN and RSC axons with blue and red light let us explore the integration of excitatory inputs in single layer 3 neurons. We compared excitatory postsynaptic potentials evoked by ATN or RSC axon photostimulation to responses when both sets of axons were activated at the same time (dual; Fig. 4A). On average, for 11 cells tested, dual oEPSPs (synchronous light onset, Fig. 4A-C) had significantly higher amplitudes than the calculated summed amplitudes of single oEPSPs (Dual/summed amplitude 2.06 ± 0.55 mV, n = 11, p = 0.0068, Wilcoxon test). Charge transfer, quantified as the surface under the dual oEPSP, was greater than the summed surfaces of single oEPSPs (Dual/summed surface 2.21 ± 0.54 mV.s, n = 11, p = 0.0098, Wilcoxon test). We note variability between individual neurons, including linear (3/11) or sublinear (1/11) summation of responses to ATN and RSC axon photostimulations in a minority of cases. Dynamic responses to repetitive stimulations were also transformed by dual photostimulation. The amplitudes for 5 consecutive dual oEPSPs were higher than for a linear summation (20 Hz, Amplitude, p = 0.0117; Fig. 4E) and charge transfer, quantified as the surface under the 5 oEPSPs, summed supralinearly most of the time (20 Hz, Surface, p = 0.0128, Two-way ANOVA; Figure 4F). Trains of dual ATN and RSC fiber stimulations also showed increased integrals under the summed oEPSPs for consecutive stimuli, compared to the stimulation of either one or the other set of fibers alone, indicating stronger excitation over time (Fig. 4E, F). Taken together, these data show supralinear summation of ATN and RSC inputs in certain single layer 3 pyramidal cells, and also a facilitation of dynamic responses to repetitive inputs at 20 Hz.

We next asked how efficiently ATN and RSC inputs would lead to action potential firing in the postsynaptic layer 3 neurons. Firing probability was higher for dual than for single input stimulation at a membrane potential of -65 mV (ATN 0.008 vs Dual 0.268, n = 5, p = 0.0216, RSC 0.024 vs Dual 0.268, n = 5, p = 0.1195, Friedman's and Dunn's tests) and higher still at -55 mV (Fig. 4G, H). The probability to initiate action potentials increased over a narrow window of time delays between stimulation of the two inputs (Fig. 4I, J). It was most likely for delays of -2 to +5 ms, with a maximum at +1 ms (RSC precedes ATN).

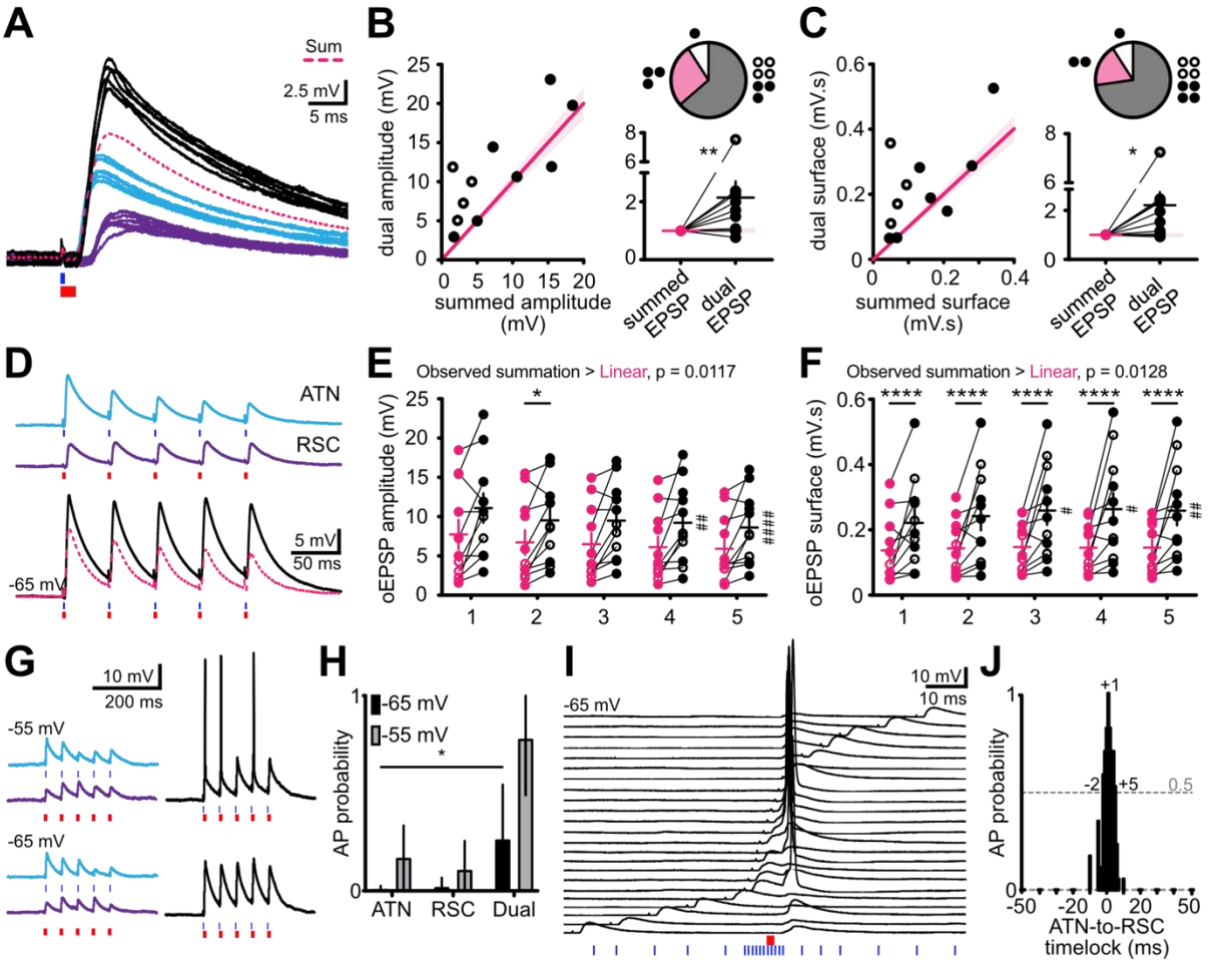

Figure 4. Supralinear summation in the subthreshold regime and action potential firing in layer 3 neurons for coincident photostimulation of ATN and RSC axons.

A, Excitatory postsynaptic responses in layer 3 neurons to independent dual wavelength photostimulation of ATN (blue light, cerulean traces) or RSC axons (red light, purple traces) or both (blue and red light, black traces). The calculated average sum of subthreshold oEPSPs evoked by separately stimulating ATN or RSC axons is indicated in pink (broken line). Records from cell 1, Fig 3D.

B, C, Amplitude (B) and integral (C) of dual oEPSPs plotted as a function of the calculated average sum of ATN and RSC oEPSPs (*left*). Each circle is a recorded L3 cell (n=11), Pink line (± 10%) indicates linearity. Pie charts summarize the number of tested neurons with supralinear (grey), linear (pink) or sublinear (white) summation. oEPSPs normalized to linear sum (*bottom right*). Solid circle, Chronos in ATN/Chrimson in RSC, empty circle, Chronos in RSC/Chrimson in ATN. * $p < 0.05$, ** $p < 0.01$, from Wilcoxon test.

D, oEPSPs induced by 20 Hz trains of ATN (light blue), RSC (purple) or dual (black) stimuli. The calculated average sum of oEPSPs evoked by separate ATN and RSC photostimulation is indicated in pink (broken line).

E, F, Amplitude (E) and integral (F) of dual subthreshold oEPSPs compared to the calculated average sum of ATN and RSC oEPSPs, for each postsynaptic response to a train of 5 stimulations at 20 Hz. Two-way ANOVA statistical p value is indicated on top of the graph. * $p < 0.05$, **** $p < 0.0001$, Šidák's multiple comparison test. # $p < 0.05$, ## $p < 0.01$, Friedman's and *post-hoc* Dunn's test.

G, Excitatory postsynaptic responses to photostimulation of ATN (blue light, cerulean traces) or RSC axons (red light, purple traces) or both (blue and red light, black traces) at resting membrane potential (-65 mV) and at a depolarized holding potential (-55 mV). Synaptic excitation may lead to action potential firing if the threshold is reached, shown here for dual blue and red photostimulation at a depolarized holding potential of -55 mV.

H, Action potential (AP) probability for either or both stimuli at -65 and -55 mV.

I, Responses to stimulating ATN fibers (blue light) and RSC fibers (red light) with varying time differences from -40 to +40 ms.

J, AP firing probability is maximal for short delays between -2 to +5 ms.

Synaptic integration of excitatory inputs may become supralinear following the activation of NMDA receptors or voltage dependent intrinsic currents that may amplify EPSPs (Fricker and Miles, 2000), especially if synaptic inhibition is reduced. To examine the factors contributing to membrane potential non-linearities, layer 3 pyramidal neurons were recorded using a Cesium-based internal solution to favor potential cationic amplifying currents, and containing QX314 to prevent action potential firing (Fig. 5). Photostimulation evoked oEPSPs of 10.9 ± 2.0 mV amplitude for ATN fibers (n = 3) and 13.7 ± 2.5 mV for RSC fibers (n = 3). The response dynamics to 5 light pulses at 20 Hz were moderately facilitating (2nd vs 1st amplitude ratio: ATN 1.39, RSC 1.17; 5th vs 1st: ATN 1.18, RSC 1.20; n = 3). The coincident activation of the two afferent fibers gave rise to supralinear oEPSP summation, and our recording conditions revealed the capacity of layer 3 pyramidal neurons to generate an all-or-none active signal. Dual photoactivation induced a large depolarization on the second or third stimulus (2nd vs 1st amplitude ratio: 1.52; 5th vs 1st: 2.90; n = 3 cells, Fig. 5A). It may be mediated by VGCC or a QX-314 resistant Na+ inward current (Fricker et al., 2009). This component appeared with higher probability and shorter latency in the presence of $GABA_A$ receptor blocker gabazine (Fig. 5B). The NMDA receptor antagonist APV largely abolished the dual EPSP amplification initially (Fig. 5C, black trace; 2nd vs 1st integral ratio: 1.22; 5th vs 1st: 1.32), but amplification was partially restored when RSC stimulation intensity was increased (pale pink trace). NMDA receptor activation thus assists depolarization towards the activation threshold of a voltage-dependent process. It may contribute to supra-linear EPSP integration, but is not the only charge carrier for non-linear EPSP amplification.

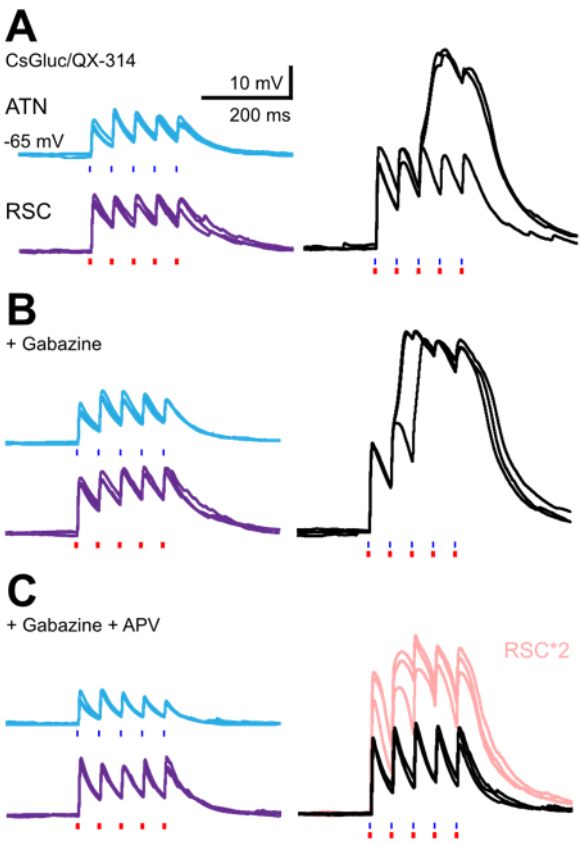

Figure 5. Postsynaptic all-or-none boosting of dual oEPSPs in layer 3 pyramidal neurons.

A, Responses of layer 3 pyramidal neurons to stimulation of ATN axons (blue light, cerulean traces), RSC axons (red light, purple traces) and both (blue and red light, black traces). Recordings were carried out at resting membrane potential (-65 mV). Recording pipette contained a cesium based internal solution and the Na^+ channel blocker QX-314, revealing a large all–or-none EPSP amplification on the third dual stimulation of a 20 Hz train.

B, In the presence of the $GABA_A$ receptor antagonist gabazine (10 µM), EPSP amplification appears earlier in the train.

C, In the additional presence of NMDA receptor antagonist APV (100 µM), dual EPSP amplifications were abolished (black trace). Amplification was partially restored by an increased RSC stimulation intensity (pale pink traces).

Recruitment of presubicular layer 4 neurons by ATN and RSC afferents

Presubicular layer 4 neurons are intrinsic bursting pyramidal neurons that project to the lateral mammillary nucleus (Huang et al., 2017). This pathway is critical for the coordinated stable landmark control of HD cells in the thalamus and throughout the HD cell circuit (Yoder et al., 2015). To investigate the input connectivity of layer 4 principal cells, we recorded the responses from these neurons following stimulations of ATN and RSC afferents.

Layer 4 neurons labeled by retrograde tracers injected in the lateral mammillary nucleus were located in the *lamina dissecans* of the presubiculum, below layer 3, where thalamic axons ramify (Fig. 6A-D). The apical dendrites of layer 4 pyramidal neurons extended towards presubicular layer 1 as previously described (Huang et al., 2017), but they mostly circumvented layer 3, by swerving towards the adjacent subiculum, avoiding the thalamic afferents. The apical dendrite of some neurons would cross obliquely through layer 3, while some others detoured the thalamic afferents in layer 3 entirely (Fig. 6C, D, Supp. Fig. 7, 8). Layer 4 neurons had a more depolarized resting membrane potential, lower input resistance and time constant than layer 3 neurons. A characteristic voltage sag developed during hyperpolarizing steps, indicative of a prominent I_h current. A comparison of intrinsic passive and active membrane properties for layer 3 and 4 neurons is given (Supp. Fig. 9). Importantly, layer 4 neurons discharged bursts of two or three action potentials at the onset of a depolarizing step current injection, followed by regular action potentials. Rebound burst firing could be triggered after the offset of a hyperpolarizing step (Fig. 6E). Burst firing was abolished by the T-type Ca^{2+} channel blocker TTA-P2 (Fig. 6F).

We next recorded the synaptic excitation layer 4 neurons received following the optical activation of thalamic or RSC afferents. Responses were compared to those of layer 3 pyramidal neurons (Fig. 6G). Overall, latencies of oEPSCs in layer 4 neurons were longer than for layer 3 (ATN layer 4, 6.2 ± 0.6 ms, n = 8, vs. layer 3, 2.4 ± 0.2 ms, n = 24; RSC layer 4, 5.6 ± 0.4 ms, n = 9, vs. layer 3, 2.9 ± 0.2 ms, n = 27; Fig. 6H), indicating possible polysynaptic excitation of layer 4 neurons. Bath application of TTX-4AP did not abolish oEPSPs entirely, leaving a low amplitude component with short, potentially monosynaptic latencies (latency ATN 3.9 ± 0.6 ms, RSC 2.9 ± 0.2 ms, n = 5; Fig. 6I).

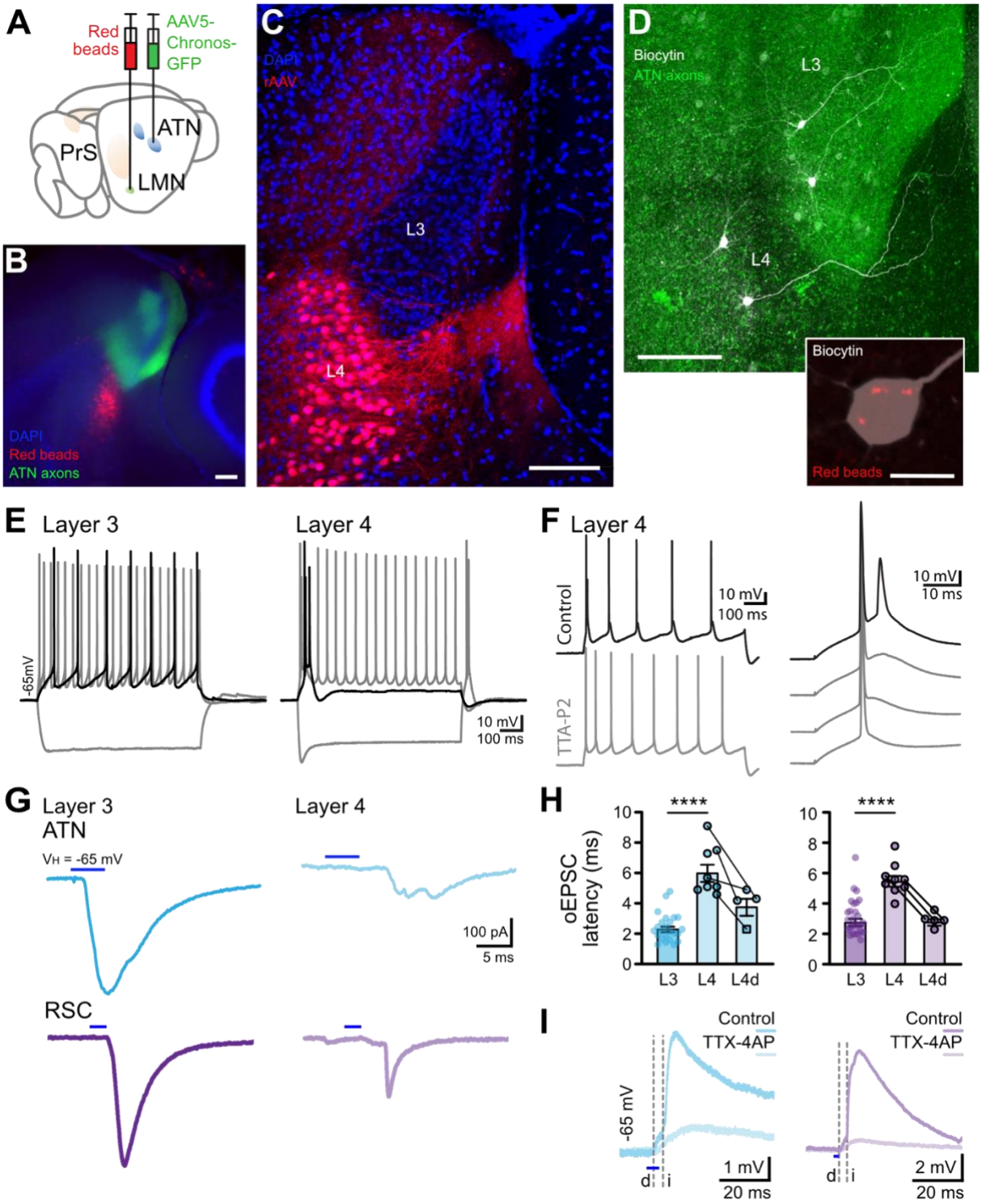

Figure 6. LMN-projecting layer 4 bursting neurons are indirectly recruited by thalamic and retrosplenial inputs.

A, AAV-Chronos-GFP was injected in the anterior thalamus and red retrobeads in the LMN.

B, Thalamic axons (*green*) targeting superficial layers 1 and 3 of presubiculum. Retrobeads label layer 4 LMN-projecting neurons.

C, Retrograde labeling by AAV2retro. Apical dendrites of layer 4 pyramidal neurons avoid L3 where thalamic axons ramify.

D, Two layer 3 and two L4 neurons filled with biocytin (white), surrounded by GFP thalamic afferents (green). Scale bar 100 µm. Inset, retrobeads (red) in the soma of a LMN-projecting layer 4 neuron. Scale bar 10 µm.

E, Representative firing pattern of layer 3 and layer 4 neurons. Grey traces represent responses to injection of

hyperpolarizing and depolarizing current pulses. Black trace shows the neuronal response at rheobase.
F, Responses to depolarizing current injection of layer 4 neuron in control conditions or in presence of TTA-P2 (1 µM), a blocker of T-type Ca^{2+} channels (*left*), and evolution of the burst firing in presence of TTA-P2 which progressively abolished burst and underlying calcium current.
G. Voltage-clamp responses to stimulation of ATN or RSC inputs with blue light.
H, oEPSC latency for layer 3 and layer 4 cells for ATN or RSC inputs. Same cells are indicated by connecting line.
I, Current-clamp responses to stimulation of ATN inputs in control conditions and in presence of TTX-4AP. Dashed lines indicate the timing of monosynaptic (d, direct) and disynaptic (i, indirect) components of the response.

The temporal relationship between the excitation received by neurons from layer 3 and 4 was compared directly in simultaneous double recordings. We compared the onset latency of layer 4 neurons oEPSPs to the onset and peak of layer 3 APs (Fig 7A-C). The oEPSP onset in the layer 4 neuron occurred after the AP peak of the layer 3 neuron, for ATN (4/5) or RSC (1/1) photostimulation. When the layer 3 neuron was depolarized via the patch pipette, action potentials were initiated, but no excitatory postsynaptic events were detected in the simultaneously recorded L4 neuron, indicating that the recorded L3-L4 cell pairs were not synaptically connected pairs. Nevertheless, considering that layer 3 neurons are the recipient of the thalamic and retrosplenial signals in the presubiculum, these data suggest that information flows from ATN or RSC afferents via layer 3 neurons, to layer 4 neurons.

To examine the efficiency of dual photostimulation of ATN and RSC fibers to drive layer L4 cells to action potential firing, pairs of layer 3 and 4 neurons were recorded in slices from Chronos/ATN and Chrimson/RSC double injected mice (n = 3 pairs; Fig. 7D-H). Layer 3 neurons responded with precisely timed action potentials to low intensity (0.25 mW) blue light stimulation of ATN axons, while simultaneously recorded layer 4 neurons responded with barely detectable oEPSPs. Increasing the excitatory drive by adding red light to activate RSC axons increased the amplitude and reliability of oEPSPs evoked in layer 4 neurons. Photostimulation with high intensity light pulses that activated ATN axons and RSC axons ultimately evoked bursts of action potentials, with the activation of an underlying Ca^{2+} current (Fig. 7E). It seems likely that the increased recruitment of layer 3 neurons by strong (and non-specific) illumination of ATN and RSC axons was required to produce sufficient excitation in layer 4 to reach action potential threshold. We note that not only dual photostimulation initiates spiking in layer 4. The vigorous activation of a single set of afferent fibers can also strongly recruit layer 3 neurons and subsequently lead to action potentials in layer 4 neurons, as apparent in recordings from mice where only one afferent brain area, ATN or RSC, expressed an opsin (Supp. Fig. 10). Taken together, we suggest that layer 3 neurons act as a necessary relay of the ATN and RSC inputs onto LMN-projecting layer 4 pyramidal neurons. However, we failed to demonstrate a functional synaptic connection between layer 3 to layer 4 neurons in n = 8 paired recordings, and neither did we reveal any putative synaptic contacts between filled axons of layer 3 and dendrites of layer 4 cells. On the other hand, we did find a possible synaptic connection between two neighboring L4 neurons (Fig 7F, G), with a close apposition between axon and dendrite. The probability for L4-L4 synapses in slices may be higher than the probability to preserve L3-L4 synapses. Recurrent excitation may promote bursting in layer 4 neurons, and pharmacological evidence indicates NMDA receptor related EPSP amplification favors bursting propensity (Fig. 7H).

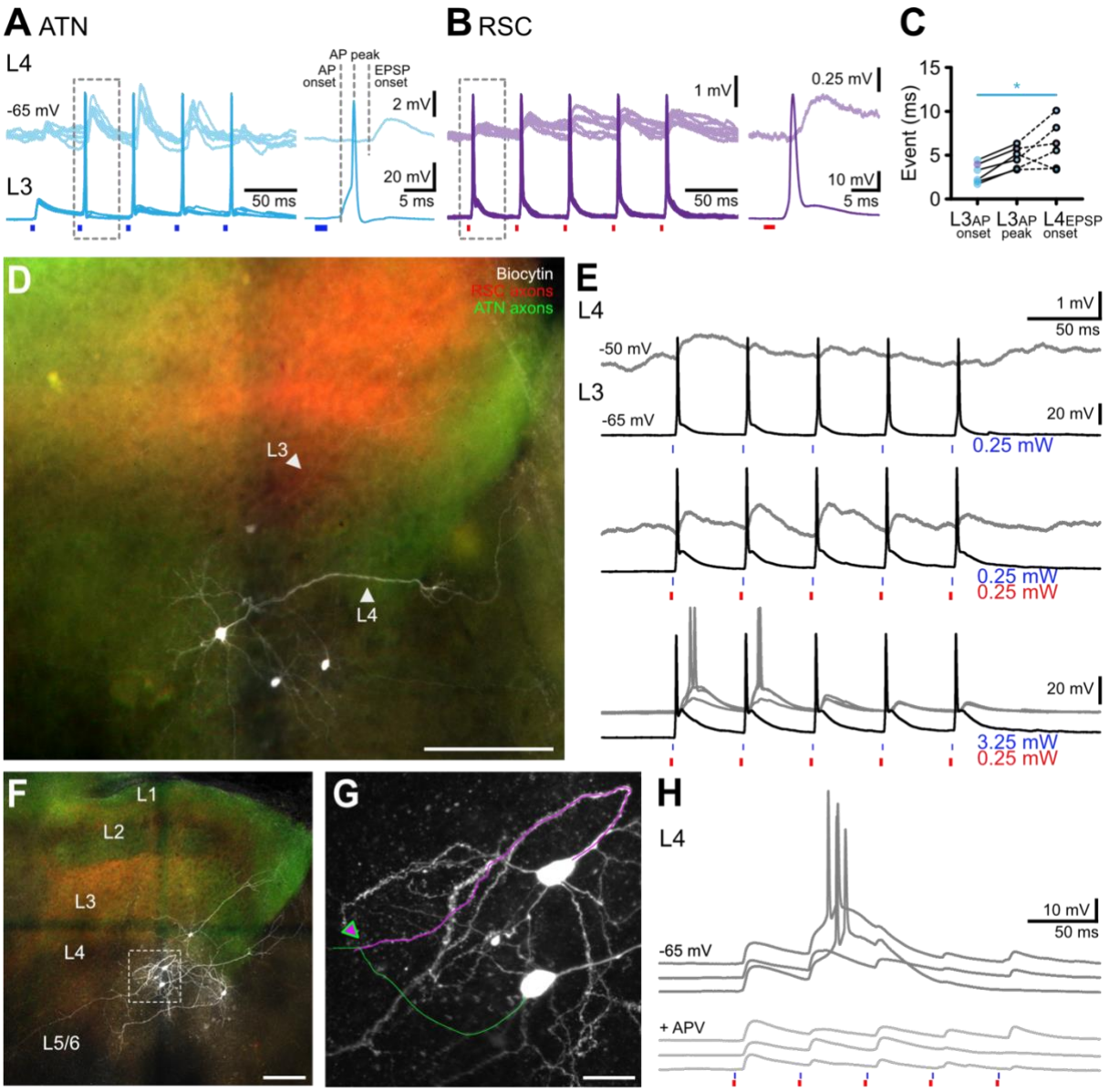

Figure 7. Transsynaptic activation of LMN projecting neurons in layer 4.

A, Simultaneous records of layer 3 (lower) and 4 (upper) neurons during photostimulation of ATN afferents. EPSP onset is delayed in L4 neurons. Right panel is a close-up view of the squared area.

B, Simultaneous recording of layer 3 and 4 neurons during photostimulation of RSC afferents. As in A, L4 neurons responded with a delay. Right panel is a close-up view of the squared area.

C, Latencies of synaptic activation indicated by the dotted lines in A,B (ATN stimulation, n = 4 cells; RSC stimulation, n = 1). Full line indicates onset and peak latencies from single layer 3 neurons (n = 5). Dotted lines link to the latencies in simultaneously recorded layer 4 neurons. $p < 0.05$, Kruskal-Wallis multiple comparison test.

D, Biocytin labeled layer 3 and 4 neurons surrounded by thalamic (*green*) and retrosplenial (*red*) axons. Layer 4 apical dendrite crosses layer 3 for a short distance before arborizing outside of ATN targeted area, towards the subiculum. Scale bar, 100µm.

E, Simultaneous records from layer 4 and layer 3 cells to ATN input stimulation (*low amplitude blue*), ATN and RSC (*blue and red, light intensities compatible with independent photostimulation*) or non-specific ATN and RSC (*high amplitude blue and red*) in a Chronos/ATN - Chrimson/RSC double injected mouse.

F, Same configuration as in D. Dotted square is enlarged in G. Scale bar, 100µm.

G, Enlarged confocal image showing a potential synaptic contact between two layer 4 neurons. Pink, the apical dendrite of this L4 neuron makes a U-turn, away from layer 3, where the thalamic axons ramify. Green, axon of

a neighboring L4 neuron. Its apical dendrite extends toward L3 initially, then quickly leaves the thalamo-recipient L3 to the right, towards the subiculum. Scale bar 20µm

H, Bursts of action potentials evoked by dual stimulation of ATN and RSC were abolished by NMDA receptor antagonist APV.

Discussion

Understanding where and how HD attractor signals become anchored to visual landmarks offers a window for unraveling principles underlying the process of matching external information from the environment to internally generated brain dynamics. We have identified the cell-type specific integration of thalamic and cortical long-range afferents underlying this computation, and find that in the presubiculum, visuo-spatial integration and HD updating is a two-stage process. Using anatomical and physiological techniques combined with dual wavelength optogenetics in mice, we show that layer 3 pyramidal cells of dorsal presubiculum are innervated by synapses made by ATN and RSC projections. This convergence may form the substrate for integration of HD signals relayed from the thalamus and visual landmark information from RSC. Most layer 3 pyramidal neurons received excitatory glutamatergic synapses from both ATN and RSC fibers, that may be segregated on different dendrites, or close to each other on the same dendritic branches. Independent optogenetic stimulation of these inputs revealed nonlinear membrane potential dynamics for nearly coincident EPSPs which facilitated firing in a narrow time window. Single neuron computation, inhibitory gating and a precise subcellular synapse distribution, provides complexity and flexibility in the integration by layer 3 pyramidal cells of head direction and landmark signals. LMN-projecting layer 4 neurons are di-synaptically recruited by thalamic and retrosplenial afferents through layer 3 neurons, adding an additional layer of processing, before transmitting a visual updating signal to LMN through bursts of action potentials.

Anatomical convergence of ATN and RSC projections in the dorsal Presubiculum

Fibers from the ATN and RSC have been shown to project to the presubiculum. Retrograde tracing in this study demonstrates that these two areas provide the strongest projections to this area (Fig. 1). Anterior thalamic fibers (Van Groen et Wyss 1990c; 1990a; 1990b; 1992; Shibata et Honda 2012; Vogt et Miller 1983) ramify in and delimit the anatomical borders of the presubiculum (Liu et al., 2021; Simonnet et al., 2017). HD signals from the thalamus drive presubicular HD neurons (Goodridge and Taube, 1997) by synapses made directly with layer 3 pyramidal cells (Nassar et al., 2018). We found the highest density of retrogradely labeled cell bodies was located in dorsal and ventral regions of the ipsilateral anterior thalamus. The retrosplenial cortex stood out as the most strongly labeled cortical region innervating the presubiculum. We detected retrogradely transported beads in cells of layers 2 and 5 of dysgranular RSC, and layer 5 of the granular RSC across its antero-posterior axis (Sugar and Witter, 2016).

We examined the anatomy and physiology of these two afferent systems to ask how visual landmark signals from the RSC are combined with HD signals relayed via the ATN. Anterograde fiber tracing, with an AAV5 construct expressing Chronos-GFP, confirmed that axons from both regions project to superficial layers of the dorsal presubiculum. No RSC projections were found in ventral PrS for injections in rostral RSC, as previously noted (Jones and Witter 2007; Kononenko and Witter 2012).

Both RSC and ATN innervated superficial presubicular layers 1 and 3, while sparing layer 2 containing somata of calbindin positive neurons (Fig. 1K and cf. Balsamo et al. 2022). The anatomical fine structure revealed microzones containing a high density of ATN-positive fibers, but not RSC fibers, in upper layer 3.

Pathway specific functional connectivity onto PrS layer 3 neurons.

Photostimulation of GFP-Chronos expressing axons let us compare synaptic events initiated in layer 3 pyramidal cells by fibers from the ATN or the RSC in dorsal presubiculum slices (Fig. 2). Both ATN and RSC afferents formed mono-synaptic connections based on latencies and confirmed pharmacologically. Synapses for both projections were glutamatergic, dependent on NMDA and AMPA receptors. The amplitudes of synaptic currents varied, with an overall similar amplitude distribution for ATN and RSC stimulation. This may be due to variable expression levels (Hooks et al. 2015), or it could indicate an uneven distribution of coupling weights across cells. ATN and RSC fiber mediated EPSCs depressed during repetitive activation at 20 Hz. EPSPs induced firing early during repetitive stimulation. RSC inputs tended to produce more sustained EPSP dynamics and slower rise times than ATN afferents for low intensity stimulation. ATN synapses with presubicular pyramidal cells resemble those made by thalamic afferents in the somatosensory cortex - high release with depressing dynamics, (Gil et al., 1999) possibly due to presynaptic expression of VGLut2 (Liu et al., 2021).

Dual wavelength optogenetic stimulation was used to study interactions between ATN and RSC afferents that contacted single layer 3 pyramidal cells. This approach permitted independent excitation of intermingled axons expressing blue-light sensitive Chronos and red-shifted Chrimson, in ATN or RSC fibers respectively (Klapoetke et al., 2014). Precautions were taken to avoid cross-stimulation since all channelrhodopsin variants are somewhat sensitive to blue light. With the fast, sensitive opsin Chronos expressed in ATN fibers, synaptic events were induced by very short (0.5 ms), low intensity, 0.25 mW, stimuli. For RSC fibers expressing Chrimson, using light stimuli of duration 2 ms, adjusting intensity up to 2 mW initiated synaptic events of comparable amplitude. Our calibration experiments (Supp Fig. 6) provided strong evidence for the independence of responses. While Chrimson has slower dynamics than Chronos (Klapoetke et al., 2014), synaptic events induced by stimulating either opsin were similar, as shown by inverting the two opsin variants injected in ATN and RSC fibers respectively (Fig. 4).

This dual opsin approach permitted independent stimulation with blue and red light pulses. Most (76%) recorded layer 3 neurons generated synaptic events in response to stimulation of both ATN and RSC fibers providing a substrate for integration of landmark information from the RSC with thalamic HD signals. Nearly coincident inputs (-2 to +5 ms separation, Figure 5D) were most effective to trigger firing. This seems of particular interest as there is a high degree of coherence between AD and RSC HD representations (Fallahnezhad et al., 2023), and spikes in these two regions may be produced in close temporal relation (< 5ms; van der Goes et al. 2022). Converging inputs from thalamic and retrosplenial axons can therefore excite common postsynaptic presubicular layer 3 neurons with very short delays, such that presubicular detection of coincidence may serve to enhance the head direction signal that is sent to the MEC. Response dynamics to combined stimulation of both inputs at 20 Hz were maintained or facilitating, compared to the more depressing dynamics of repetitive stimulations of one set of afferent fibers. Combined and temporally precise inputs from ATN and RSC may thus help maintain HD signaling during immobility.

Nonlinear signal integration in layer 3 thalamo-recipient neurons

The convergent connectivity patterns of ATN and RSC axons onto single layer 3 pyramidal cells provides the anatomical basis of synaptic integration. Putative synaptic contacts from both afferent fiber systems were found on the basal dendrites of pyramidal cells (Fig. 6), sometimes on the same branch. Photostimulation centered on the soma of recorded neurons predominantly activated synapses on basal dendrites. A local spike-generating mechanism could confer supralinearity if the activated synapses were located on a same dendritic branch (Poirazi and Papoutsi, 2020; Polsky et al., 2004). Clustered synapses could also guide the formation of new spines and synapses during integration of landmark information in the HD signal. Learning might bind new inputs into functional synaptic clusters (Hedrick et al., 2022). From our small sample of three layer 3 pyramidal cells we find that both ATN and RSC axons target basal dendrites, and more RSC than ATN axons made contacts with apical dendrites (Fig. 4). It would be interesting to test effects of precise, near coincident activation of basal and apical synapses, but our data permit no conclusions on this point. Distinct dendritic inputs to layer 3 cells may improve spatial perception (Takahashi et al., 2016) enhancing HD signal quality by integration with landmark information.

Our data show EPSP amplification upon coincident ATN and RSC activations is assisted by NMDA receptor activation and voltage gated inward dendritic currents above a certain threshold (Figure 4G; Fricker et al. 2009). The absence of inhibition facilitated EPSP amplification for coincident inputs (Figure 4), indicating that disinhibition may be permissive for supralinearity and gate firing by dynamic modulation of the balance between inhibition and excitation (Milstein et al., 2015). VIP expressing interneurons and their excitation by cholinergic neuromodulation could provide such disinhibition of the presubicular microcircuit (Porter et al., 1999; Slomianka and Geneser, 1991). A supervisory when-to-learn signal for HD updating in the presubiculum might function analogously to the dopamine promoting associations between sensory cues and head direction cells in the fly compass neurons (Fisher et al., 2022). It is however unclear whether LTP type learning takes place in the mammalian head direction circuit. Presubicular layer 3 specifically lacks the GluR1 subunit of AMPA receptors (Martin et al 1993; Ishihara et al 2016) that is critical for LTP expression (Boehm et al 2006). The absence of GluR1 might indicate that the thalamo-presubicular synapses in layer 3 function without classical long term plasticity.

Layer 3 pyramidal cells may be described as multi-compartmental computational devices (Häusser et Mel 2003; Mel 1993; Poirazi, Brannon, et Mel 2003; Spruston 2008) which integrate HD and landmark information. ATN axons drive presubicular HD neurons (Peyrache et al. 2015) and RSC mixed selectivity neurons contribute visual landmark information and allocentric spatial references (Jacob et al. 2017; Mitchell et al. 2018; Vann, Aggleton, et Maguire 2009). NMDA mediated dendritic spikes enhance tuning selectivity in the visual cortex (Smith et al. 2013; Wilson et al. 2016) and in the barrel cortex (Lavzin et al. 2012). In the dorsal presubiculum, they might enable binding of visual landmarks with HD tuning. It is tempting to speculate that nonlinear synaptic integration and inhibitory gating may be involved in flexibly updating the allocentric direction of HD cells based on the integration of visual landmark information to the current HD signal. In the primary sensory cortex, nonlinearities are known to increase perceptual threshold of sensory information (Takahashi et al. 2016; 2020). The attractor network could thus be either stabilized or flexibly reset to external spatial cues.

Function significance of two-layer processing preceding projection to LMN

Global updating of the HD signal involves the Presubiculum-to-LMN projection via the bursting layer 4 neurons. LMN projecting neurons in layer 4 are positioned such that their dendrites overlap little with thalamic and retrosplenial axons, granting partial isolation from direct excitation, and

permitting a second level of integration of information from layer 3 neurons. Indeed layer 3 axons cross to layer 4 where they may connect layer 4 neurons basal dendrites. Layer 4 pyramidal neurons are recruited following a strong enough excitatory input from layer 3 that may or may not lead to action potential initiation. What might be the computational advantage of segregating the integration of converging input signals from the updating signal across layers? Such an arrangement can reconcile the need for immediate transmission of an integrated signal to the medial entorhinal cortex, and a transformation of the integrated signal into bursts of actions potentials that conveys a strong message to upstream HD circuit elements. The two-stage system includes a synaptic threshold mechanism that allows for gated, conditional updating. Our results suggest that layer 4 cells may form a recurrent system, even though the extent to which this may be the case is unclear. Functionally, layer 4 neurons are uniquely positioned to update the HD signal in the LMN with visual landmark information. Our study provides new microcircuit evidence that supports and expands on the findings of Yoder et al. (2015). We clarify how the thalamic HD signal is relayed to the grid cell system in the medial entorhinal cortex and transformed into bursting information received in the LMN.

Limitations

Burst firing may play a role for learning in hierarchical circuits (Naud et al., 2023; Payeur et al., 2021). In the HD circuit, visual landmark information contained in bursts might cause a reset or anchoring of the HD attractor in the LMN and beyond. How bursting information is received in LMN remains to be examined. Presubiculum might not be the only brain area where HD signals are updated, but it uniquely provides a feed-back projection from a cortical HD structure back to the mammillary nucleus. A further investigation of the specific role of the layer 3 to layer 4 transmission is warranted, and the link to spatial perception and behavioural updating needs to be strengthened.

Acknowledgements

This work is supported by the Centre National de la Recherche Scientifique and the Université Paris Cité. DF received funding from the Agence Nationale de la Recherche (ANR-DFG Program, ANR-18-CE92-0051 BURST), from the ERA-NET NEURON Program (ANR-20-NEUR-0005 VELOSO), and the FLAG-ERA HBP Program (ANR-21-HBPR-0002 VIPattract). This work has benefited from support by the BioMedTech Facilities at Université Paris Cité (Institut National de la Santé et de la Recherche Médicale Unité S36/Unité Mixte de Service 2009). We thank Richard Miles for helpful comments on the manuscript.

References

Alexander AS, Nitz DA (2015) Retrosplenial cortex maps the conjunction of internal and external spaces. Nat Neurosci 18:1143–1151.

Auger SD, Mullally SL, Maguire EA (2012) Retrosplenial Cortex Codes for Permanent Landmarks. PLOS ONE 7:e43620.

Balsamo G, Blanco-Hernández E, Liang F, Naumann RK, Coletta S, Burgalossi A, Preston-Ferrer P (2022) Modular microcircuit organization of the presubicular head-direction map. Cell Rep 39.

Blair HT, Sharp PE (1995) Anticipatory head direction signals in anterior thalamus: evidence for a thalamocortical circuit that integrates angular head motion to compute head direction. J Neurosci 15:6260–6270.

Boccara CN, Sargolini F, Thoresen VH, Solstad T, Witter MP, Moser EI, Moser M-B (2010) Grid cells in pre- and parasubiculum. Nat Neurosci 13:987–994.

Calton JL, Stackman RW, Goodridge JP, Archey WB, Dudchenko PA, Taube JS (2003) Hippocampal place cell instability after lesions of the head direction cell network. J Neurosci 23:9719–9731.

Clark BJ, Bassett JP, Wang SS, Taube JS (2010) Impaired Head Direction Cell Representation in the Anterodorsal Thalamus after Lesions of the Retrosplenial Cortex. J Neurosci 30:5289–5302.

Fallahnezhad M, Le Mero J, Zenelaj X, Vincent J, Rochefort C, Rondi-Reig L (2023) Cerebellar control of a unitary head direction sense. Proc Natl Acad Sci U S A 120:e2214539120.

Fisher YE, Marquis M, D'Alessandro I, Wilson RI (2022) Dopamine promotes head direction plasticity during orienting movements. Nature 612:316–322.

Fricker D, Dinocourt C, Eugène E, Wood JN, Wood J, Miles R (2009) Pyramidal cells of rodent presubiculum express a tetrodotoxin-insensitive Na+ current. J Physiol 587:4249–4264.

Gil Z, Connors BW, Amitai Y (1999) Efficacy of thalamocortical and intracortical synaptic connections: quanta, innervation, and reliability. Neuron 23:385–397.

Goodridge JP, Taube JS (1997) Interaction between the postsubiculum and anterior thalamus in the generation of head direction cell activity. J Neurosci 17:9315–9330.

Hedrick NG, Lu Z, Bushong E, Singhi S, Nguyen P, Magaña Y, Jilani S, Lim BK, Ellisman M, Komiyama T (2022) Learning binds new inputs into functional synaptic clusters via spinogenesis. Nat Neurosci 25:726–737.

Huang L-W, Simonnet J, Nassar M, Richevaux L, Lofredi R, Fricker D (2017) Laminar Localization and Projection-Specific Properties of Presubicular Neurons Targeting the Lateral Mammillary Nucleus, Thalamus, or Medial Entorhinal Cortex. eneuro 4:ENEURO.0370-16.2017.

Jacob P-Y, Casali G, Spieser L, Page H, Overington D, Jeffery K (2017) An independent, landmark-dominated head-direction signal in dysgranular retrosplenial cortex. Nat Neurosci 20:173–175.

Jones BF, Witter MP (2007) Cingulate cortex projections to the parahippocampal region and hippocampal formation in the rat. Hippocampus 17:957–976.

Keshavarzi S, Bracey EF, Faville RA, Campagner D, Tyson AL, Lenzi SC, Branco T, Margrie TW (2022) Multisensory coding of angular head velocity in the retrosplenial cortex. Neuron 110:532-543.e9.

Klapoetke NC et al. (2014) Independent optical excitation of distinct neural populations. Nat Methods 11:338–346.

Knierim JJ, Zhang K (2012) Attractor dynamics of spatially correlated neural activity in the limbic system. Annu Rev Neurosci 35:267–285.

Kononenko NL, Witter MP (2012) Presubiculum layer III conveys retrosplenial input to the medial entorhinal cortex. Hippocampus 22:881–895.

Liu J, Kashima T, Morikawa S, Noguchi A, Ikegaya Y, Matsumoto N (2021) Molecular characterization of superficial layers of the presubiculum during development. Front Neuroanat 15.

Mathon B, Nassar M, Simonnet J, Le Duigou C, Clemenceau S, Miles R, Fricker D (2015) Increasing the effectiveness of intracerebral injections in adult and neonatal mice: a neurosurgical point of view. Neurosci Bull 31:685–696.

McNaughton BL, Battaglia FP, Jensen O, Moser EI, Moser M-B (2006) Path integration and the neural basis of the "cognitive map." Nat Rev Neurosci 7:663–678.

Milstein AD, Bloss EB, Apostolides PF, Vaidya SP, Dilly GA, Zemelman BV, Magee JC (2015) Inhibitory Gating of Input Comparison in the CA1 Microcircuit. Neuron 87:1274–1289.

Nassar M, Simonnet J, Huang L-W, Mathon B, Cohen I, Bendels MHK, Beraneck M, Miles R, Fricker D (2018) Anterior Thalamic Excitation and Feedforward Inhibition of Presubicular Neurons Projecting to Medial Entorhinal Cortex. J Neurosci 38:6411–6425.

Naud R, Friedenberger Z, Toth K (2023) Silences, Spikes and Bursts: Three-Part Knot of the Neural Code.

Payeur A, Guerguiev J, Zenke F, Richards BA, Naud R (2021) Burst-dependent synaptic plasticity can coordinate learning in hierarchical circuits. Nat Neurosci 24:1010–1019.

Peyrache A, Lacroix MM, Petersen PC, Buzsáki G (2015) Internally organized mechanisms of the head direction sense. Nat Neurosci 18:569–575.

Poirazi P, Papoutsi A (2020) Illuminating dendritic function with computational models. Nat Rev Neurosci 1–19.

Polsky A, Mel BW, Schiller J (2004) Computational subunits in thin dendrites of pyramidal cells. Nat Neurosci 7:621–627.

Porter JT, Cauli B, Tsuzuki K, Lambolez B, Rossier J, Audinat E (1999) Selective excitation of subtypes of neocortical interneurons by nicotinic receptors. J Neurosci Off J Soc Neurosci 19:5228–5235.

Preston-Ferrer P, Coletta S, Frey M, Burgalossi A (2016) Anatomical organization of presubicular head-direction circuits. eLife 5.

Ranck JB (1984) Head direction cells in the deep layer of dorsal presubiculum in freely moving rats. Soc Neurosci Abstr.

Rees CL, Moradi K, Ascoli GA (2017) Weighing the Evidence in Peters' Rule: Does Neuronal Morphology Predict Connectivity? Trends Neurosci 40:63–71.

Richevaux L, Schenberg L, Beraneck M, Fricker D (2019) In Vivo Intracerebral Stereotaxic Injections for Optogenetic Stimulation of Long-Range Inputs in Mouse Brain Slices. JoVE J Vis Exp e59534.

Shibata H, Honda Y (2012) Thalamocortical projections of the anterodorsal thalamic nucleus in the rabbit. J Comp Neurol 520:2647–2656.

Simonnet J, Eugène E, Cohen I, Miles R, Fricker D (2013) Cellular neuroanatomy of rat presubiculum. Eur J Neurosci 37:583–597.

Simonnet J, Nassar M, Stella F, Cohen I, Mathon B, Boccara CN, Miles R, Fricker D (2017) Activity dependent feedback inhibition may maintain head direction signals in mouse presubiculum. Nat Commun 8:16032.

Simonnet J, Richevaux L, Fricker D (2021) Single or Double Patch-Clamp Recordings In Ex Vivo Slice Preparation: Functional Connectivity, Synapse Dynamics, and Optogenetics. Methods Mol Biol Clifton NJ 2188:285–309.

Sit KK, Goard MJ (2022) Coregistration of heading to visual cues in retrosplenial cortex.

Skaggs WE, Knierim JJ, Kudrimoti HS, McNaughton BL (1995) A model of the neural basis of the rat's sense of direction. Adv Neural Inf Process Syst 7:173–180.

Slomianka L, Geneser FA (1991) Distribution of acetylcholinesterase in the hippocampal region of the mouse: I. Entorhinal area, parasubiculum, retrosplenial area, and presubiculum. J Comp Neurol 303:339–354.

Stackman RW, Taube JS (1998) Firing properties of rat lateral mammillary single units: head direction, head pitch, and angular head velocity. J Neurosci 18:9020–9037.

Sugar J, Witter MP (2016) Postnatal development of retrosplenial projections to the parahippocampal region of the rat. eLife 5.

Takahashi N, Oertner TG, Hegemann P, Larkum ME (2016) Active cortical dendrites modulate perception. Science 354:1587–1590.

Taube JS (1995) Head direction cells recorded in the anterior thalamic nuclei of freely moving rats. J Neurosci 15:70–86.

Taube JS, Muller RU, Ranck JB (1990a) Head-direction cells recorded from the postsubiculum in freely moving rats. I. Description and quantitative analysis. J Neurosci 10:420–435.

Taube JS, Muller RU, Ranck JB (1990b) Head-direction cells recorded from the postsubiculum in freely moving rats. II. Effects of environmental manipulations. J Neurosci 10:436–447.

Van der Goes M-SH, Voigts J, Newman JP, Toloza EHS, Brown NJ, Murugan P, Harnett MT (2022) Coordinated Head Direction Representations in Mouse Anterodorsal Thalamic Nucleus and Retrosplenial Cortex.

Van Groen T, Wyss JM (2003) Connections of the retrosplenial granular b cortex in the rat. J Comp Neurol 463:249–263.

Van Groen T, Wyss JM (1992) Connections of the retrosplenial dysgranular cortex in the rat. J Comp Neurol 315:200–216.

Van Groen T, Wyss JM (1990a) The connections of presubiculum and parasubiculum in the rat. Brain Res 518:227–243.

Van Groen T, Wyss JM (1990b) Connections of the retrosplenial granular a cortex in the rat. J Comp Neurol 300:593–606.

Van Groen T, Wyss JM (1990c) The postsubicular cortex in the rat: characterization of the fourth region of the subicular cortex and its connections. Brain Res 529:165–177.

Vogt BA, Miller MW (1983) Cortical connections between rat cingulate cortex and visual, motor, and postsubicular cortices. J Comp Neurol 216:192–210.

Yoder RM, Peck JR, Taube JS (2015) Visual landmark information gains control of the head direction signal at the lateral mammillary nuclei. J Neurosci 35:1354–1367.

Yoder RM, Taube JS (2011) Projections to the anterodorsal thalamus and lateral mammillary nuclei arise from different cell populations within the postsubiculum: implications for the control of head direction cells. Hippocampus 21:1062–1073.

Yoder RM, Valerio S, Crego ACG, Clark BJ, Taube JS (2019) Bilateral postsubiculum lesions impair visual and nonvisual homing performance in rats. Behav Neurosci 133:496–507.

Zugaro MB, Arleo A, Berthoz A, Wiener SI (2003) Rapid spatial reorientation and head direction cells. J Neurosci 23:3478–3482.